Decentralized Stability Certificates in IBR-Dominated Grids: The Role of the Network State

Zhimeng Wang[1], Sushobhan Chatterjee[1], Sijia Geng[1], Richard Pates[2], Enrique Mallada[1]

[1] *Johns Hopkins University* [2] *Lund University*

Suggested Citation

Z. Wang, S. Chatterjee, S. Geng, R. Pates, and E. Mallada, "Decentralized Stability Certificates in IBR-Dominated Grids: The Role of the Network State," in *Proceedings of the PowerUp Conference*, 2026.

BibTeX Entry

```
@inproceedings{wang2026decentralizedstabili,
  author = {Wang, Zhimeng and Chatterjee, Sushobhan and Geng, Sijia and Pates,
      Richard and Mallada, Enrique},
  title = {Decentralized Stability Certificates in {IBR}-Dominated Grids: The Role
      of the Network State},
  booktitle = {Proceedings of the PowerUp Conference},
  year = {2026},
}
```

Decentralized Stability Certificates in IBR-Dominated Grids: The Role of the Network State

Zhimeng Wang†, Sushobhan Chatterjee†, Sijia Geng†, Richard Pates‡, Enrique Mallada†

***Abstract*—Small-signal instabilities, such as unforced sub-synchronous oscillations (SSOs), are increasingly observed in inverter-based resource (IBR) dominated grids. While decentralized stability certificates offer a scalable means to avoid instability onset, they are typically derived under restrictive network-state assumptions–such as small angle differences or negligible voltage drops–that cannot capture how departures from these conditions affect system stability. In this paper, we develop a network model and a decentralized analysis framework that explicitly characterizes how reactive power mismatches, line loading, and inverter control parameters jointly determine small-signal stability. We show that increased steady-state reactive power mismatches and line loading lead to more stringent conditions on admissible inverter droop gains. These results make decentralized stability certificates explicitly network-state dependent, showing how network stress shrinks the set of stabilizing local controller parameters.**

***Index Terms*—Decentralized stability, inverter-based resources, passivity, reactive power, small-signal stability.**

I. Introduction

Small-signal instabilities are becoming increasingly prevalent in inverter-based resource (IBR) dominated grids, often manifesting as unforced sub-synchronous oscillations (SSOs) [1]. Such instabilities have been reported across a wide range of scenarios, including weak-grid conditions, controller misconfigurations at commissioning, and post-contingency network reconfigurations [2], [3]. While some events can be explained by classical resonance phenomena or control-structure interactions [4], the precise mechanisms driving many of these oscillations remain poorly understood. In particular, instabilities often arise spontaneously, without a clear disturbance or topological trigger, underscoring the need for improved analytical tools that capture how the underlying network state shapes small-signal dynamics and stability-margins [5].

Recent research has emphasized the use of *decentralized certificates* to ensure small signal stability [6]–[11]. These approaches derive scale-free conditions that guarantee stability under bounded uncertainty, offering scalable alternatives to full electromagnetic transient (EMT) simulations and global eigenvalue analyses [6]. To obtain such tractable, decentralized conditions, most formulations either adopt simplifying network steady-state assumptions–such as small phase differences [7], [11], near-uniform voltage magnitudes [8], or active–reactive decoupling [6], [9]–or implicitly encode network-state dependence within the local linearization of inverter models [10]. As a result, the dependence of stability margins on the network state is either neglected, implicitly confined to a nominal regime, or absorbed into model abstractions.

In this paper, we develop a network model and accompanying analysis framework that derives decentralized stability certificates without imposing explicit or implicit assumptions on the network state. The port-based representation and loop-transformation perspective used in our framework are inspired by the scalable decentralized stability framework in [12], which develops local stability protocols for heterogeneous networks. Our approach relies on a small-signal model in which lines and IBRs are represented as multi-port components, interconnected through an incidence-matrix-based network structure. In particular, each transmission line is modeled as a quasi-stationary multi-port subsystem mapping small deviations of nodal angles and voltages to directional real and reactive power flows, while inverter dynamics are represented through filtered droop gains. This explicit port-based decomposition makes the passivity properties of individual components–and potential violations thereof–transparent, enabling a systematic and decentralized application of loop transformation techniques to compensate for non-passive effects.

Applying this framework reveals an intrinsic coupling between the network steady state and the admissible control gains required for guaranteeing small-signal stability. In particular, our results show that increasing reactive power asymmetries $(Q_{ij} - Q_{ji})$ or line loading–captured through larger phase differences $(\theta_{ij} = \theta_i - \theta_j)$–progressively restrict the set of stabilizing voltage droop gains. These findings align with the well-established notion that small-signal stability depends on the operating point of the network, and indicate that decentralized certificates derived under nominal or lightly stressed conditions can be overly optimistic when applied to stressed operating regimes. Moreover, the derived conditions provide practical guidance for preserving stability by indicating when network-aware control retuning or operational redispatch may be required. Though independently derived, our results closely relate to the earlier work [13]. Understanding the full extent of the connection with our work is left as future work.

The rest of the paper is organized as follows. Section II reviews the preliminary tools used throughout the paper, including the passivity stability theorem and loop transformation techniques for analyzing feedback interconnections. Section III introduces the network and device models and describes their interconnection through a structured feedback representation. Section IV presents the main decentralized stability certificate and provides a detailed proof of the result. Section V demonstrates the implications of the proposed conditions through an illustrative numerical example. Finally, Section VI summarizes the main findings and discusses their implications for decentralized stability analysis and inverter-based grid operation.

†Zhimeng Wang, Sushobhan Chatterjee, Sijia Geng, Enrique Mallada are with the Department of Electrical and Computer Engineering, Johns Hopkins University, Baltimore, MD, USA. Email: {zwang471, schatt21, sgeng, mallada}@jhu.edu

‡Richard Pates is with the Department of Automatic Control, Lund University, Lund, Sweden. Email: {richard.pates}@control.lth.se

II. Preliminaries

Our analysis relies on passivity theory and standard mechanisms for compensating the lack of passivity in interconnected systems. Here, we introduce passivity stability theorem, which provides sufficient conditions for the stability of feedback interconnections, and introduce loop transformation techniques that allow passivity properties to be modified through equivalent interconnection representations. These tools form the basis for the decentralized stability analysis developed in the remainder of the paper.

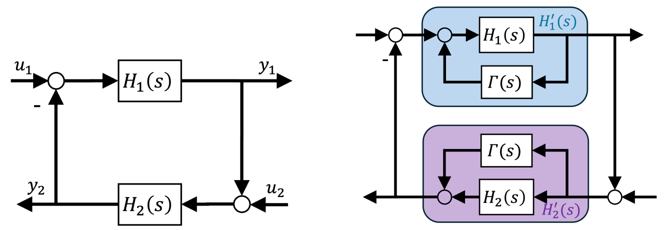

(a) Negative feedback interconnection of $H_1(s)$ and $H_2(s)$.

(b) Fig. 1a with loop transformation $\Gamma(s)$.

Fig. 1: Loop transformation.

A. Internal Feedback Stability

We consider the standard negative feedback interconnection of two square, proper transfer matrices $H_1(s)$ and $H_2(s)$. The resulting closed-loop input–output relation can be written as

$$\begin{bmatrix} y_1 \\ y_2 \end{bmatrix} = \underbrace{\begin{bmatrix} (I+H_1H_2)^{-1}H_1 & -(I+H_1H_2)^{-1}H_1H_2 \\ H_2(I+H_1H_2)^{-1}H_1 & H_2(I+H_1H_2)^{-1} \end{bmatrix}}_{=:\,H_1\#H_2(s)} \begin{bmatrix} u_1 \\ u_2 \end{bmatrix},$$

where we use I as an identity matrix with proper dimensions, and I_m as an $m \times m$ identity matrix.

Definition 1 (Internal Feedback Stability)**.** *The negative feedback interconnection of $H_1(s)$, $H_2(s)$ is said to be* internally stable *if all transfer matrices comprising $H_1\#H_2(s)$ are stable, i.e., all poles of $H_1\#H_2(s)$ lie in the open left-half plane.*

Under the assumption that there are no right-half-plane pole–zero cancellations between $H_1(s)$ and $H_2(s)$—i.e., all right-half-plane poles of $H_1(s)$ and $H_2(s)$ are contained in the minimal realizations of $H_1(s)H_2(s)$ and $H_2(s)H_1(s)$—internal stability of one closed-loop transfer matrix implies internal stability of all others [14]. This notion will be used throughout the paper.

B. Passivity Stability Theorem

We briefly review standard passivity definitions and a classical passivity-based stability theorem for feedback interconnections.

Definition 2 (Passivity)**.** *A square, proper, real rational transfer matrix $H(s)$ is* passive *if:*

i. $H(s)$ has poles in $\Re(s) \le 0$.

ii. The Hermitian part of $H(j\omega)$ is positive semidefinite for any ω for which $j\omega$ is not a pole:

$$H(j\omega) + H^*(j\omega) \succeq 0.$$

iii. Any pole on the imaginary axis is simple, and its residue

$$R = \lim_{s \to j\omega_0} (s - j\omega_0)H(s)$$

is Hermitian positive semidefinite.

The transfer matrix is strictly passive *if inequalities in $i.$ and $ii.$ are strict.*

Theorem 1 (Feedback Stability via Passivity)**.** *Consider the standard negative feedback interconnection of two systems $H_1(s)$ and $H_2(s)$ with compatible dimensions. The closed-loop system is internally stable if the following conditions hold:*

i. System $H_1(s)$ is passive, and system $H_2(s)$ is strictly passive.

ii. The loop gain magnitude at infinite frequency satisfies the small-gain condition:

$$\bar{\sigma}\left(H_1(j\infty)\right)\bar{\sigma}\left(H_2(j\infty)\right) < 1.$$

Proof. The proof of this Theorem is standard. For completeness we provide a proof in Appendix A. □

C. Loop Transformation

We will use loop transformations to compensate the lack of passivity in transmission lines, allowing in this way to apply Theorem 1. When doing this, one needs to ensure that the internal stability of the loop-shifted system implies the internal stability of the original system. We address this issue with the following two lemmas.

Lemma 1 (Corollary 5.5 in [15])**.** *Suppose $H_1(s)$ is stable. Then system $H_1(s)\#H_2(s)$ is internally stable iff $\left[I + H_2(s)H_1(s)\right]^{-1} H_2(s)$ is stable.*

Lemma 2 (Loop transformation internal stability equivalence)**.** *Let $H_1(s)$ and $H_2(s)$ be proper real-rational transfer matrices with compatible dimensions, and let $\Gamma(s)$ be a stable proper transfer matrix of compatible dimension. Suppose that*

$$\det(I - \Gamma(s)H_1(s)) \not\equiv 0,$$

and define

$$H_1'(s) := H_1(s)\left(I - \Gamma(s)H_1(s)\right)^{-1}, \quad H_2'(s) := H_2(s) + \Gamma(s).$$

Assume that $H_1'(s)$ is proper real-rational and stable. Assume also that $H_1(s)$ is stable and that

$$\det(I + H_2(\infty)H_1(\infty)) \neq 0, \quad \det(I + H_2'(\infty)H_1'(\infty)) \neq 0.$$

Then $H_1(s)\#H_2(s)$ is internally stable if and only if $H_1'(s)\#H_2'(s)$ is internally stable.

Proof. See Appendix B. □

Remark 1 (Necessity of Lemma 2)**.** *A classical approach to address the equivalence of internal stability of loop-transformed systems usually requires no pole-zero cancellations on the* closed *right-half plane [16]. Unfortunately, the* *proposed system in this paper has a pole-zero cancellation on the imaginary axis, rendering this approach not applicable. We make an emphasis on the requirement of* closed *as some literature rather state it as* open *[14] [15].*

III. Network Model

In this section, we develop a first principle-based small-signal model of the IBRs and the transmission network, and then connect them to construct an interconnection.

A. Inverter-Based Resource (IBR) Model

We model each IBR as a grid-forming (GFM) device that regulates frequency through active power feedback and voltage magnitude through reactive power feedback. Let ΔP_i and ΔQ_i denote the incremental active and reactive power injected by inverter i into the network, and let $\Delta\omega_i$ and $\Delta \ln|v_i|$ denote the incremental frequency and logarithmic voltage magnitude at bus i.

We adopt the standard sign convention in which positive power corresponds to injection into the grid, and the inverter control uses the *negative* of these quantities as feedback inputs. The small-signal inverter dynamics are modeled by

$$\begin{bmatrix}\Delta\omega_i\\ \Delta\ln|v_i|\end{bmatrix} = G_i(s)\begin{bmatrix}-\Delta P_i\\ -\Delta Q_i\end{bmatrix},$$

where the transfer matrix

$$G_i(s) := \begin{bmatrix}\frac{k_{p,i}}{\tau_{\omega,i}s+1} & 0\\ 0 & \frac{k_{q,i}}{\tau_{v,i}s+1}\end{bmatrix},$$

$k_{p,i}, k_{q,i} > 0$ are the active power–frequency droop gain and reactive power-voltage droop gain, respectively. $\tau_{\omega,i}, \tau_{v,i} > 0$ are the frequency and voltage control time constants, respectively.

We define

$$\begin{bmatrix}-\Delta P\\ -\Delta Q\end{bmatrix} := \begin{bmatrix}-\Delta P_1\\ -\Delta Q_1\\ \vdots\\ -\Delta P_n\\ -\Delta Q_n\end{bmatrix} \in \mathbb{R}^{2n}, \begin{bmatrix}\Delta\omega\\ \Delta\ln|v|\end{bmatrix} := \begin{bmatrix}\Delta\omega_1\\ \Delta\ln|v_1|\\ \vdots\\ \Delta\omega_n\\ \Delta\ln|v_n|\end{bmatrix} \in \mathbb{R}^{2n}$$

as the input and output signals of the IBR devices. Thus the dynamics of all the inverters concatenated is characterized by

$$\begin{bmatrix}\Delta\omega\\ \Delta\ln|v|\end{bmatrix} = G(s)\begin{bmatrix}-\Delta P\\ -\Delta Q\end{bmatrix}, \tag{1}$$

where $G(s) = \text{blkdiag}\left(G_1(s), \cdots, G_n(s)\right)$.

B. Line Model

Consider a lossless transmission line $e = \{i, j\}$ connecting buses i and j. Let

$$v_i = |v_i|e^{j\theta_i}, \qquad v_j = |v_j|e^{j\theta_j}, \qquad \theta_{ij} := \theta_i - \theta_j$$

denote the steady-state voltage phasors and phase difference. The line is modeled as purely inductive with inductance L_e, and we define the normalized susceptance $b_e := \frac{1}{\omega_0 L_e}$, where ω_0 is the synchronous angular frequency.

The steady-state complex power injected from bus i into the line is

$$S_{ij} := P_{ij} + jQ_{ij} = v_i\, i_{ij}^*,$$

with $i_{ij} = jb_e(v_i - v_j)$, and S_{ji} defined analogously.

Linearizing the AC power-flow equations around the operating point yields a quasi-stationary, port-based small-signal model of the line,

$$\begin{bmatrix}\Delta P_{ij}\\ \Delta Q_{ij}\\ \Delta P_{ji}\\ \Delta Q_{ji}\end{bmatrix} = N_e(s)\begin{bmatrix}\Delta\omega_i\\ \Delta\ln|v_i|\\ \Delta\omega_j\\ \Delta\ln|v_j|\end{bmatrix},$$

where the line transfer matrix admits the factorization

$$N_e(s) = J_e\,\text{diag}\left(\frac{1}{s}, 1, \frac{1}{s}, 1\right).$$

We introduce the notation $W_n(s) = \text{diag}\left(\frac{1}{s}, 1, \ldots, \frac{1}{s}, 1\right) \in \mathbb{C}^{n\times n}$, thus $N_e(s) = J_e W_4(s)$. The integrator terms arise from the kinematic relation $\dot{\theta}_k = \omega_k$, while the static gain matrix $J_e := b_e|v_i||v_j|\,\bar{J}_e$ captures the steady-state sensitivity of line power flows to voltage magnitudes and phase differences, and the normalized Jacobian $\bar{J}_e \in \mathbb{R}^{4\times 4}$ is given by

$$\bar{J}_e = \begin{bmatrix}\cos\theta_{ij} & \sin\theta_{ij} & -\cos\theta_{ij} & \sin\theta_{ij}\\ \sin\theta_{ij} & 2\frac{|v_i|}{|v_j|} - \cos\theta_{ij} & -\sin\theta_{ij} & -\cos\theta_{ij}\\ -\cos\theta_{ij} & -\sin\theta_{ij} & \cos\theta_{ij} & -\sin\theta_{ij}\\ \sin\theta_{ij} & -\cos\theta_{ij} & -\sin\theta_{ij} & 2\frac{|v_j|}{|v_i|} - \cos\theta_{ij}\end{bmatrix}.$$

Let $E = \{e_1, \ldots, e_m\}$ denote the set of transmission lines. Stacking the incremental nodal variables and line power flows over all lines, we define

$$\begin{bmatrix}\Delta\omega_E\\ \Delta\ln|v_E|\end{bmatrix} := \begin{bmatrix}\Delta\omega_{i_1}\\ \Delta\ln|v_{i_1}|\\ \Delta\omega_{j_1}\\ \Delta\ln|v_{j_1}|\\ \vdots\\ \Delta\omega_{i_m}\\ \Delta\ln|v_{i_m}|\\ \Delta\omega_{j_m}\\ \Delta\ln|v_{j_m}|\end{bmatrix}, \qquad \begin{bmatrix}\Delta P_E\\ \Delta Q_E\end{bmatrix} := \begin{bmatrix}\Delta P_{i_1j_1}\\ \Delta Q_{i_1j_1}\\ \Delta P_{j_1i_1}\\ \Delta Q_{j_1i_1}\\ \vdots\\ \Delta P_{i_mj_m}\\ \Delta Q_{i_mj_m}\\ \Delta P_{j_mi_m}\\ \Delta Q_{j_mi_m}\end{bmatrix}.$$

The concatenated line dynamics can then be written compactly as

$$\begin{bmatrix}\Delta P_E\\ \Delta Q_E\end{bmatrix} = N_E(s)\begin{bmatrix}\Delta\omega_E\\ \Delta\ln|v_E|\end{bmatrix}, \tag{2}$$

where

$$N_E(s) = \text{blkdiag}\big(N_{e_1}(s), \ldots, N_{e_m}(s)\big) = J_E\, W_{4m}(s),$$

with $J_E := \text{blkdiag}(J_{e_1}, \ldots, J_{e_m})$.

C. Interconnection Model

To connect the bus vector signals and the line-end vector signals, we introduce the matrix

$$M := \begin{bmatrix}M_{e_1} & M_{e_2} & \cdots & M_{e_m}\end{bmatrix} \in \{0,1\}^{2n\times 4m},$$

where for each line,

$$M_e = \begin{bmatrix}e_i & e_j\end{bmatrix} \otimes I_2 \in \{0,1\}^{2n\times 4},$$

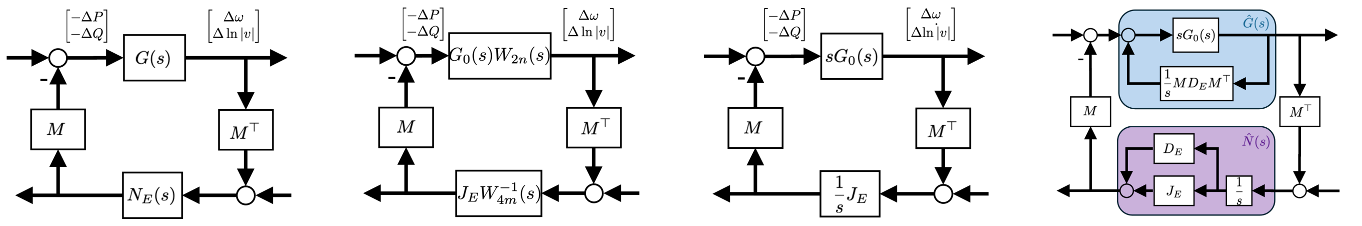

(a) System $G(s)\#_M N_E(s)$. (b) $G_0(s)W_{2n}(s)\#_M J_E W_{4m}^{-1}(s)$. (c) System $sG_0(s)\#_M \frac{1}{s}J_E$. (d) System $\hat{G}(s)\#_M \hat{N}(s)$.

Fig. 2: Systems for stability analysis.

and e_k is the k-th standard basis vector.

Therefore, the bus vector signals and the line-end vector signals can be related as

$$\begin{bmatrix}\Delta\omega_E\\ \Delta\ln|v_E|\end{bmatrix} = M^\top \begin{bmatrix}\Delta\omega\\ \Delta\ln|v|\end{bmatrix}, \quad \begin{bmatrix}\Delta P\\ \Delta Q\end{bmatrix} = M\begin{bmatrix}\Delta P_E\\ \Delta Q_E\end{bmatrix} \quad (3)$$

Equations (1), (2), and (3) provide a compact first-principles description of the full networked system, in which the inverter dynamics and the line dynamics are interconnected exclusively through the operators $M^\top$ (node-to-edge) and M (edge-to-node). This port-based representation is inspired by the network decomposition framework in [12], where heterogeneous components are represented through local input-output ports and coupled through structured interconnection operators. We denote this interconnection between systems G and N_E via M and $M^\top$ as $G\#_M N_E$. This structure will be the basis for the passivity and stability analysis in the sequel.

IV. Decentralized Stability Certificate

We now present and prove the main result of this paper.

A. Main Result

Theorem 2 (Decentralized Stability Certificate)**.** *Consider the device and network models in* (1)*,* (2)*, and* (3)*, interconnected as $G(s)\#_M N_E(s)$ in Fig. 2a. Assume that the operating point satisfies $\cos\theta_{ij} > 0$ for all $\{i,j\} \in E$. If the following condition holds: For each line $e = \{i,j\} \in E$,*

$$\begin{aligned}&\left(2\frac{d_e}{b_e|v_i||v_j|} - \frac{2}{\cos\theta_{ij}}\right)\sqrt{\left(\frac{Q_{ij}-Q_{ji}}{b_e|v_i||v_j|}\right)^2+4}\\ &+\left(\frac{d_e}{b_e|v_i||v_j|}\right)^2 - \frac{2}{\cos\theta_{ij}}\frac{d_e}{b_e|v_i||v_j|}+4 \geq 0,\end{aligned} \quad (4)$$

where $\sum_{e:i\in e} d_e = \frac{1}{k_{q,i}}$. Then $G(s)\#_M N_E(s)$ is internally stable.

B. Proof of Main Theorem

We prove Theorem 2 by following the flow chart in Fig. 3.

1) Notation setup: To facilitate the stability analysis, we normalize the system parameters around the operating point. For each line $e = \{i,j\}$, define

$$\theta_e := \theta_{ij}, \qquad c_{\theta_e} := \cos\theta_e, \qquad s_{\theta_e} := \sin\theta_e.$$

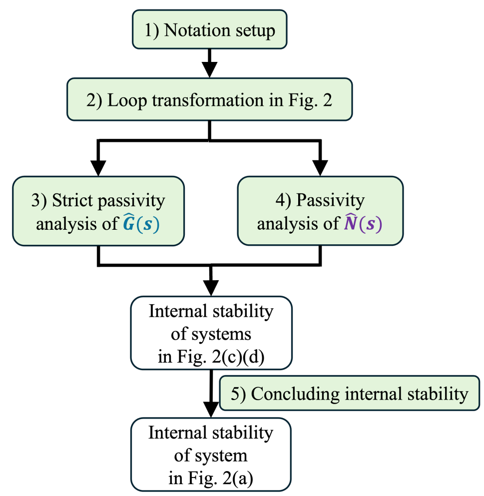

Fig. 3: Flow chart of the proof of Theorem 2. The colored blocks represent the steps.

Furthermore, inspired by [12], we introduce the normalized gain and the corresponding diagonal matrix

$$\bar{d}_e := \frac{d_e}{b_e|v_i||v_j|}, \qquad \bar{D}_e = \mathrm{diag}(0, \bar{d}_e, 0, \bar{d}_e),$$

to be used in our loop transformation, and the normalized reactive power flow p_{ij}, q_{ij} and q_{ji}

$$p_{ij} := \frac{P_{ij}}{b_e|v_i||v_j|}, \qquad q_{ij} := \frac{Q_{ij}}{b_e|v_i||v_j|}, \qquad q_{ji} := \frac{Q_{ji}}{b_e|v_i||v_j|}.$$

Also notice the standard power-flow identities of lossless lines

$$p_{ij} = \sin\theta_{ij}, \qquad q_{ij} - q_{ji} = \frac{Q_{ij}-Q_{ji}}{b|v_i||v_j|} = \frac{|v_i|}{|v_j|} - \frac{|v_j|}{|v_i|}.$$

We will prove our results using the following coordinates

$$\Sigma := \frac{|v_i|}{|v_j|} + \frac{|v_j|}{|v_i|} + \bar{d}_e = \sqrt{(q_{ij}-q_{ji})^2+4} + \bar{d}_e, \quad (5)$$

$$\Delta := \frac{|v_i|}{|v_j|} - \frac{|v_j|}{|v_i|} = q_{ij} - q_{ji}. \quad (6)$$

2) Loop transformation: The map in (2) is in general not passive, as J_E is in general not positive semidefinite. To facilitate the subsequent analysis, we consider the systems in Fig. 2, in which Fig. 2a is the original system, and can be equivalently expressed as in Fig. 2b, where

$$G_0(s) = \mathrm{blkdiag}\left(\begin{bmatrix}\frac{k_{p,i}}{s(\tau_{\omega,i}s+1)} & 0\\ 0 & \frac{k_{q,i}}{\tau_{v,i}s+1}\end{bmatrix}\right),$$

and $G_0(s)$ characterizes the dynamics

$$\begin{bmatrix}\Delta\theta \\ \Delta \ln|v|\end{bmatrix} = G_0(s)\begin{bmatrix}-\Delta P \\ -\Delta Q\end{bmatrix}.$$

In Fig. 2c, $G'(s) := sG_0(s)$ characterizes the dynamics

$$\begin{bmatrix}\Delta\omega \\ \Delta \dot{\ln|v|}\end{bmatrix} = G'(s)\begin{bmatrix}-\Delta P \\ -\Delta Q\end{bmatrix}. \tag{7}$$

For each $e = \{i, j\}$, we choose loop shifting parameter $d_e \geq 0$, and apply the corresponding loop shifting matrix D_E to the line dynamics in Fig. 2c, which yields the loop shifted interconnection in Fig. 2d. On the IBR side, this loop transformation induces the additional nodal positive feedback $\frac{1}{s}K\begin{bmatrix}\Delta\omega \\ \Delta \dot{\ln|v|}\end{bmatrix}$, where $K := M\, D_E\, M^\top$. By construction, K is diagonal and acts only on the voltage-magnitude channels:

$$K = \operatorname{diag}(0, \kappa_1, 0, \kappa_2, \ldots, 0, \kappa_n),$$

where $\kappa_i = \sum_{e:i\in e} d_e$. Note that D_e acts locally on each line, whereas K aggregates these effects at the nodal level.

3) Strict passivity analysis of loop shifted devices $\hat{G}(s)$: The diagonal term $\frac{1}{s}K$ is equivalent to introducing, at each bus i, a local positive feedback in the $\dot{\ln|v_i|}$ channel with gain κ_i.

Given the IBR dynamics in (7), the additional feedback κ_i/s acts as a positive feedback around the first-order system $\frac{k_{q,i}s}{\tau_{v,i}s+1}$ in the voltage channel. Consequently, the effective voltage-channel dynamics become

$$\frac{k_{q,i}s}{\tau_{v,i}s + 1 - \kappa_i k_{q,i}},$$

which remains *strictly* passive with $\kappa_i = \frac{1}{k_{q,i}}$.

4) Passivity analysis of loop shifted lines $\hat{N}(s)$: With the loop transformation introduced, each of the line transfer function $\frac{1}{s}J_e$ can be replaced by the shifted map

$$\frac{1}{s}J_e \;=\; \frac{1}{s}(J_e + D_e) \;-\; \frac{1}{s}D_e.$$

Equivalently, we define the *passivized* line block

$$\bar{N}_{\ln,e}(s) := \frac{1}{s}\,(J_e + D_e), \qquad N_{D,e}(s) := \frac{1}{s}\,D_e,$$

so that the original line is decomposed into a passive candidate $\bar{N}_{\ln,e}$ and a diagonal integrator $N_{D,e}$. Since $\frac{1}{s}$ is positive real, a sufficient condition for $\bar{N}_{\ln,e}(s)$ to be passive is $\bar{J}_e + \bar{D}_e \succeq 0$, and is a simple semidefinite condition on d_e.

Stacking over all lines gives the passivized stacked line map

$$\bar{N}_{\ln}(s) = \frac{1}{s}\,(J_E + D_E), \qquad N_D(s) = \frac{1}{s}\,D_E.$$

For each line, define $H_e := \bar{J}_e + \bar{D}_e$, giving

$$H_e = \begin{bmatrix} c_{\theta_e} & s_{\theta_e} & -c_{\theta_e} & s_{\theta_e} \\ s_{\theta_e} & 2\frac{|v_i|}{|v_j|} - c_{\theta_e} + \bar{d}_e & -s_{\theta_e} & -c_{\theta_e} \\ -c_{\theta_e} & -s_{\theta_e} & c_{\theta_e} & -s_{\theta_e} \\ s_{\theta_e} & -c_{\theta_e} & -s_{\theta_e} & 2\frac{|v_j|}{|v_i|} - c_{\theta_e} + \bar{d}_e \end{bmatrix}. \tag{8}$$

The definition in (5)–(6) can be equivalently written as

$$2\frac{|v_i|}{|v_j|} + \bar{d}_e = \Sigma + \Delta, \qquad 2\frac{|v_j|}{|v_i|} + \bar{d}_e = \Sigma - \Delta.$$

To analyze the definiteness of H_e, we apply a congruence transformation $\tilde{H}_e := T^\top H_e T$ that transforms the basis into Σ and Δ, thereby block-diagonalizing the matrix and simplifying the stability check. We pick

$$T := \begin{bmatrix} 1 & 0 & 1 & 0 \\ 0 & 1 & 0 & 1 \\ 1 & 0 & -1 & 0 \\ 0 & 1 & 0 & -1 \end{bmatrix}.$$

Applying the transformation to (8) and simplifying yields

$$\tilde{H}_e = \begin{bmatrix} 0 & 0 & 0 & 0 \\ 0 & 2\Sigma - 4c_{\theta_e} & 4s_{\theta_e} & 2\Delta \\ 0 & 4s_{\theta_e} & 4c_{\theta_e} & 0 \\ 0 & 2\Delta & 0 & 2\Sigma \end{bmatrix},$$

thus $H_e \succeq 0$ is equivalent to $G_e \succeq 0$, and is further equivalent to $\hat{G}_e := \frac{1}{2}G_e \succeq 0$, where

$$G_e := \begin{bmatrix} 2\Sigma - 4c_{\theta_e} & 4s_{\theta_e} & 2\Delta \\ 4s_{\theta_e} & 4c_{\theta_e} & 0 \\ 2\Delta & 0 & 2\Sigma \end{bmatrix}, \hat{G}_e = \begin{bmatrix} \Sigma - 2c_{\theta_e} & 2s_{\theta_e} & \Delta \\ 2s_{\theta_e} & 2c_{\theta_e} & 0 \\ \Delta & 0 & \Sigma \end{bmatrix} \succeq 0.$$

We assume $c_{\theta_e} > 0$, so the middle diagonal entry $2c_{\theta_e}$ is strictly positive. Then $\hat{G}_e \succeq 0$ is equivalent to the Schur complement of the middle block being PSD:

$$S_e := \begin{bmatrix} \Sigma - 2c_{\theta_e} & \Delta \\ \Delta & \Sigma \end{bmatrix} - \frac{1}{2c_{\theta_e}}\begin{bmatrix} 2s_{\theta_e} \\ 0 \end{bmatrix}\begin{bmatrix} 2s_{\theta_e} & 0 \end{bmatrix} = \begin{bmatrix} \Sigma - 2c_{\theta_e} - \frac{2s_{\theta_e}^2}{c_{\theta_e}} & \Delta \\ \Delta & \Sigma \end{bmatrix},$$

it is PSD iff its diagonals and determinant are nonnegative.

We substitute Σ and Δ into (4), thus the condition ensures

$$-\Delta^2 + \Sigma^2 - \frac{2\Sigma}{c_{\theta_e}} = \Sigma^2 - 2c_{\theta_e}\Sigma - \frac{2s_{\theta_e}^2}{c_{\theta_e}}\Sigma - \Delta^2 = \det(S_e) \geq 0 \tag{9}$$

Moreover, (9) guarantees

$$\Sigma^2 - \frac{2}{c_{\theta_e}}\Sigma \geq \Delta^2 \geq 0 \;\Rightarrow\; \Sigma\left(\Sigma - \frac{2}{c_{\theta_e}}\right) \geq 0.$$

Since $\Sigma \geq 0$, this implies $\Sigma \geq \frac{2}{c_{\theta_e}}$, i.e., (9) implies the smallest diagonal element in S_e is nonnegative.

In conclusion, the condition ensures S_e is PSD, implying that $\hat{G}_e$, G_e and H_e are PSD, which further implies the passivity of the loop-shifted lines.

5) Concluding internal stability: Given that the condition ensures the strict passivity of the loop shifted IBRs and the passivity of the loop shifted lines, the loop-shifted system $\hat{G}(s)\#_M\hat{N}(s)$ in Fig. 2d is internally stable. Since $sG_0(s)$ is stable and there is no RHP pole-zero cancellation between $sG_0(s)$ and $\frac{1}{s}J_E$, we apply Lemma 2 and conclude that system $sG_0(s)\#_M\frac{1}{s}J_E$ is also internally stable, i.e., signals $(\Delta P, \Delta Q, \Delta\omega, \Delta \dot{\ln|v|}) \to 0$ as $t \to \infty$. To further show that $\Delta \ln|v| \to 0$ as $t \to \infty$, which can be implied by the internal stability of the original system $G(s)\#_M N_E(s)$ in Fig. 2a, we adapt the proof method from [11] and state the following.

Lemma 3. *Consider system $G(s)\#_M N_E(s)$ in Fig. 2a, and system $\hat{G}(s)\#_M\hat{N}(s)$ in Fig. 2d. Then, internal feedback stability of the minimal realization of all four closed-loop transfer functions of the loop-shifted system $\hat{G}(s)\#_M\hat{N}(s)$ implies internal feedback stability of $G(s)\#_M N_E(s)$.*

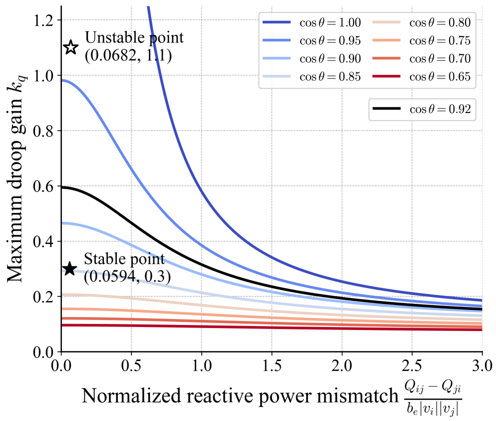

Fig. 4: $\cos\theta$ level sets illustrating how the maximum droop gain varies with $\frac{Q_{ij}-Q_{ji}}{b_e|v_i||v_j|}$. For each level set, the stable region encloses the origin.

Proof. See Appendix C. □

V. Numerical Example

We consider a two-bus system composed of two GFM inverters interconnected by a single transmission line. To validate the proposed stability certificates, we adopt a third-order nonlinear GFM model, as detailed in Appendix D, whose linearization yields (1). We begin by linearizing the nonlinear dynamics around a stable equilibrium point obtained with the following parameter settings: $p_1^* = -4$ p.u., $p_2^* = 4$ p.u., $q_1^* = 1.2$ p.u., $q_2^* = 0.5$ p.u., $k_{p,1} = k_{p,2} = 1.8$ p.u., $k_{q,1} = k_{q,2} = 0.3$ p.u., and $\omega_b = 120\pi$ rad/s. These parameters are selected to represent an operating condition characterized by voltage mismatch and line loading, as summarized below.

- Grid State: $|v_1| = 1.0218$ p.u., $|v_2| = 0.9919$ p.u., and phase angle $\theta_1 = 0°$, $\theta_2 = 23.2448°$.
- Line Parameter: $b_e = 10.0$ p.u.
- Control Gains: $k_{q,1} = k_{q,2} = 0.3$.

From the above, there is $\cos\theta = 0.9188$, $\frac{Q_{ij}-Q_{ji}}{b_e|v_1||v_2|} = 0.0593$. One can verify that, with $\kappa_i = \sum_{e:i\in e} d_e = \frac{1}{k_{q,i}}$, the condition is satisfied.

In Fig. 4, we plot the maximum admissible droop gain to maintain stability versus the $\frac{Q_{ij}-Q_{ji}}{b_e|v_i||v_j|}$. The region below each curve represents the stable operating set for a given $\cos\theta$. The varying curves represent different $\cos\theta$ values. We observe a clear inverse relationship between the reactive power mismatch and the stability margin. As the mismatch increases, the maximum allowable droop gain decreases monotonically. Furthermore, the system stability margin degrades significantly with smaller $\cos\theta$. This indicates that operating points with high reactive loading and large voltage disparity require much more conservative controller tuning to ensure stability. To validate our numerical example, in Fig. 4, we highlight the stability boundary for $\cos\theta = 0.92$ and the operating point from the example with a "★". Since the operating point lies within the safe region, the system is confirmed to be stable.

Furthermore, we examine an alternative operating point obtained by setting $k_{q,1} = 1.1$ p.u., and $k_{q,2} = 1$ p.u., while keeping all other parameters unchanged. This operating point is marked with a "☆" in Fig. 4, and violates the stability conditions established in Theorem 2, thereby demonstrating the ability of the proposed certificates to correctly characterize its stability properties. Fig. 5 presents time-domain simulations that corroborate the theoretical analysis for both the stable and unstable operating points. The left panel depicts the voltage deviations, whereas the right panel illustrates the frequency synchronization dynamics. This confirms that the proposed decentralized certificate is sufficient to guarantee the dissipation of oscillation energy.

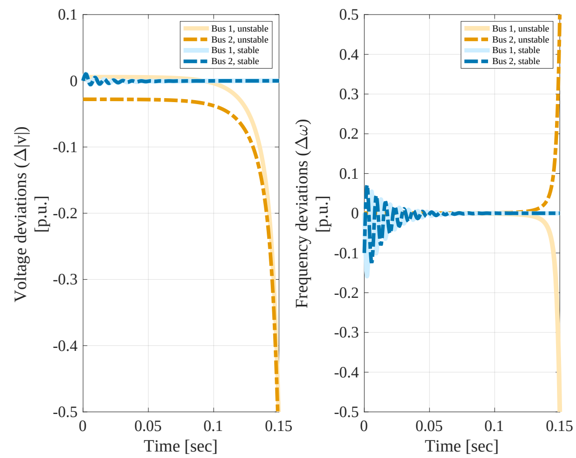

Fig. 5: Dynamic response of the 2-bus system considering one stable and one unstable scenario.

VI. Conclusion

In this paper, we present a decentralized method for certifying the small-signal stability of IBR-dominated grids, with a specific focus on the impact of reactive power flows. We demonstrate that the network's operating point is an active factor in determining local passivity. By passivizing both devices and lines using loop transformation, we derive stability criteria that are both rigorous and practically implementable. These findings offer a clearer path towards "plug-and-play" integration of IBRs, ensuring robust operation even as grid complexity and interactions increase.

VII. AI Usage Disclosure

The authors used AI tools to assist with narrative polishing, including spell-checking, visualization coding and debugging. None of the narrative was directly produced by AI; it was used solely in an advisory role and did not replace the authors. All models and ideas are the sole intellectual property of the authors, and no AI model contributed to their development.

References

[1] L. Fan, Z. Miao, S. Shah, Y. Cheng, J. Rose, S.-H. Huang, B. Pal, X. Xie, N. Modi, S. Wang, *et al.*, "Real-world 20-hz ibr subsynchronous oscillations: Signatures and mechanism analysis," *IEEE Transactions on Energy Conversion*, vol. 37, no. 4, pp. 2863–2873, 2022.

[2] Y. Li, L. Fan, and Z. Miao, “Wind in weak grids: Low-frequency oscillations, subsynchronous oscillations, and torsional interactions,” *IEEE Transactions on Power Systems*, vol. 35, no. 1, pp. 109–118, 2019.

[3] R. N. Damas, Y. Son, M. Yoon, S.-Y. Kim, and S. Choi, “Subsynchronous oscillation and advanced analysis: A review,” *IEEE Access*, vol. 8, pp. 224020–224032, 2020.

[4] J. Shair, X. Xie, L. Wang, W. Liu, J. He, and H. Liu, “Overview of emerging subsynchronous oscillations in practical wind power systems,” *Renewable and Sustainable Energy Reviews*, vol. 99, pp. 159–168, 2019.

[5] Y. Cheng, L. Fan, J. Rose, S.-H. Huang, J. Schmall, X. Wang, X. Xie, J. Shair, J. R. Ramamurthy, N. Modi, *et al.*, “Real-world subsynchronous oscillation events in power grids with high penetrations of inverter-based resources,” *IEEE Transactions on Power Systems*, vol. 38, no. 1, pp. 316–330, 2022.

[6] R. Pates and E. Mallada, “Robust scale-free synthesis for frequency control in power systems,” *IEEE Transactions on Control of Network Systems*, vol. 6, no. 3, pp. 1174–1184, 2019.

[7] P. Vorobev, S. Chevalier, and K. Turitsyn, “Decentralized stability rules for microgrids,” in *2019 American Control Conference (ACC)*, pp. 2596–2601, IEEE, 2019.

[8] J. D. Watson and I. Lestas, “Control of interlinking converters in hybrid ac/dc grids: Network stability and scalability,” *IEEE Transactions on Power Systems*, 2020.

[9] Z. Siahaan, E. Mallada, and S. Geng, “Decentralized stability criteria for grid-forming control in inverter-based power systems,” in *2024 IEEE Power & Energy Society General Meeting (PESGM)*, pp. 1–5, IEEE, 2024.

[10] L. Huang, D. Wang, X. Wang, H. Xin, P. Ju, K. H. Johansson, and F. Dörfler, “Gain and phase: Decentralized stability conditions for power electronics-dominated power systems,” *IEEE Transactions on Power Systems*, vol. 39, no. 6, pp. 7240–7256, 2024.

[11] V. Häberle, X. He, L. Huang, F. Dörfler, and S. Low, “Decentralized parametric stability certificates for grid-forming converter control,” *arXiv preprint arXiv:2503.05403*, 2025.

[12] R. T. Pates, *Scalable design rules for heterogeneous networks*. PhD thesis, 2014.

[13] J. Niehues, R. Delabays, A. Büttner, and F. Hellmann, “Small-signal stability of power systems with voltage droop,” *IEEE Transactions on Power Systems*, 2025.

[14] S. Skogestad and I. Postlethwaite, *Multivariable feedback control: analysis and design*. john Wiley & sons, 2005.

[15] K. Zhou, J. Doyle, and K. Glover, *Robust and optimal control*. Prentice Hall, 1996.

[16] J. C. Doyle, B. A. Francis, and A. R. Tannenbaum, *Feedback control theory*. Courier Corporation, 2013.

Appendix

A. Proof of Theorem 1

The internal stability of the feedback system in Fig. 1a is characterized by the following:

$$\begin{bmatrix} (I+H_2H_1)^{-1} & (I+H_2H_1)^{-1}H_2 \\ H_1(I+H_2H_1)^{-1} & H_1(I+H_2H_1)^{-1}H_2 \end{bmatrix}.$$

Given the strict passivity of H_2, it suffices to only check the stability of $H_1(I+H_2H_1)^{-1}$ [15], which is equivalent to $-1 \notin \sigma(H_2H_1)$.[1] Suppose $-1 \in \sigma(H_2H_1)$, let $v \neq \vec{0}$ be the corresponding eigenvector. Thus $-v = H_2H_1v$. It follows that

$$-v^*H_1^*v = v^*H_1^*H_2H_1v. \tag{10}$$

We take the conjugate transpose of both sides, it yields

$$-v^*H_1v = v^*H_1^*H_2^*H_1v. \tag{11}$$

Summing both sides of (10) and (11) gives

$$-v^*(H_1+H_1^*)v = v^*H_1^*(H_2+H_2^*)H_1v. \tag{12}$$

By the passivity of H_1 and strict passivity of H_2, the left hand side of (12) is nonpositive, while the right hand side is strictly positive for $v \neq \vec{0}$. Thus there is a contradiction, indicating that $-1 \notin \sigma(H_2H_1)$ for every finite frequency under consideration.

Moreover, since H_1 and H_2 are passive transfer matrices, they are proper, and hence the limits

$$H_1(j\infty) := \lim_{\omega\to\infty} H_1(j\omega), \quad H_2(j\infty) := \lim_{\omega\to\infty} H_2(j\omega)$$

exist and are finite. Let $\lambda \in \sigma(H_2(j\infty)H_1(j\infty))$. Then by condition ii,

$$|\lambda| \le \bar{\sigma}(H_2(j\infty)H_1(j\infty)) \le \bar{\sigma}(H_2(j\infty))\,\bar{\sigma}(H_1(j\infty)) < 1.$$

Therefore every eigenvalue of $H_2(j\infty)H_1(j\infty)$ has magnitude strictly less than one. In particular, $-1 \notin \sigma(H_2(j\infty)H_1(j\infty))$.

Therefore, the interconnection is internally stable given the conditions in Theorem 1.

[1] Here $\sigma(A)$ represents the set of eigenvalues of A.

B. Proof of Lemma 2

Define

$$T(s) := \big(I + H_2(s)H_1(s)\big)^{-1}H_2(s),$$
$$T'(s) := \big(I + H_2'(s)H_1'(s)\big)^{-1}H_2'(s).$$

First suppose that $H_1(s)\#H_2(s)$ is internally stable. Then $T(s)$ is stable. We show that $T'(s)$ is also stable.

$$\begin{aligned} T'(s) =& \big(I - \Gamma(s)H_1(s)\big)\big(I + H_2(s)H_1(s)\big)^{-1}\big(H_2(s) + \Gamma(s)\big) \\ =& \big(I - \Gamma(s)H_1(s)\big)\big(T(s) + \Gamma(s) - T(s)H_1(s)\Gamma(s)\big). \end{aligned}$$

Since $H_1(s)$, $T(s)$, $\Gamma(s)$ are stable, the right-hand side is a finite sum and product of stable transfer matrices. Hence $T'(s)$ is stable. Since $H_1'(s)$ is stable, Lemma 1 implies that $H_1'(s)\#H_2'(s)$ is internally stable.

Conversely, suppose that $H_1'(s)\#H_2'(s)$ is internally stable. Then $T'(s)$ is stable. The transformation is invertible, with

$$H_1(s) = H_1'(s)\big(I+\Gamma(s)H_1'(s)\big)^{-1}, \quad H_2(s) = H_2'(s) - \Gamma(s).$$

Applying the same argument with $\Gamma(s)$ replaced by $-\Gamma(s)$, we obtain

$$T(s) = \left(I + \Gamma(s)H_1'(s)\right)\left(T'(s) - \Gamma(s) + T'(s)H_1'(s)\Gamma(s)\right).$$

Since $H_1'(s)$, $T'(s)$, $\Gamma(s)$ are stable, $T(s)$ is stable. Since $H_1(s)$ is stable, Lemma 1 implies that $H_1(s)\#H_2(s)$ is internally stable.

C. Proof of Lemma 3

Since $sG_0(s)$ is stable and there is no RHP pole-zero cancellation between $sG_0(s)$ and $\frac{1}{s}J_E$, we apply Lemma 2 and conclude that system $sG_0(s)\#_M \frac{1}{s}J_E$ is also internally stable. Moreover, notice that

$$\left(I + G'\frac{1}{s}J_E\right)^{-1} G' = \mathrm{diag}(1, s, \cdots, 1, s)\cdot\left(I + GN_E\right)^{-1}G,$$

thus we can conclude the stability of $\left(I + GN_E\right)^{-1}G$ if the step response of the voltage derivatives converges to zero, i.e.,

$$\lim_{s\to 0} s\frac{1}{s}\left(I + G'\frac{1}{s}J_E\right)^{-1} G' = I \otimes \begin{bmatrix} * & 0 \\ 0 & 0 \end{bmatrix}. \tag{13}$$

To show (13), first simplify it as

$$\lim_{s\to 0}\left(I+G'\frac{1}{s}J_E\right)^{-1}G' = I\otimes\begin{bmatrix}* & 0\\ 0 & 0\end{bmatrix}.$$

We define permutation matrix

$$\mathcal{P}=\left[\frac{\mathcal{P}_u}{\mathcal{P}_l}\right]\in\{0,1\}^{2n\times 2n},$$

where

$$(\mathcal{P}_u)_{i,j}=\begin{cases}1 & \text{if } j=2i-1\\ 0 & \text{otherwise}\end{cases},\quad (\mathcal{P}_l)_{i,j}=\begin{cases}1 & \text{if } j=2i\\ 0 & \text{otherwise}\end{cases}.$$

We apply the permutation matrix $\mathcal{P}$ to the limit we want to show,

$$\lim_{s\to 0}\mathcal{P}\left(I+G'\frac{1}{s}J_E\right)^{-1}G'\mathcal{P}^\top = \mathcal{P}I\otimes\begin{bmatrix}* & 0\\ 0 & 0\end{bmatrix}\mathcal{P}^\top = \begin{bmatrix}* & 0\\ 0 & 0\end{bmatrix}. \tag{14}$$

Due to the orthogonality of $\mathcal{P}$, the LHS of (14) is equivalent to

$$\lim_{s\to 0}\left(I+G^\pi N^\pi\right)^{-1}G^\pi, \tag{15}$$

where

$$G^\pi = \mathcal{P}G'\mathcal{P}^\top = \begin{bmatrix}\operatorname{diag}\left(\frac{k_{p,i}}{\tau_{\omega,i}s+1}\right) & 0\\ 0 & \operatorname{diag}\left(\frac{k_{q,i}s}{\tau_{v,i}s+1}\right)\end{bmatrix}$$

$$N^\pi = \frac{1}{s}\mathcal{P}J_E\mathcal{P}^\top.$$

Notice that N^π contains a $1/s$ factor. We define $K^\pi = sN^\pi$ and take the limits:

$$\lim_{s\to 0}G^\pi = \begin{bmatrix}\operatorname{diag}(k_{p,i}) & 0\\ 0 & 0\end{bmatrix} := \bar{G},$$

$$\lim_{s\to 0}sN^\pi = \begin{bmatrix}K_{11} & K_{12}\\ K_{21} & K_{22}\end{bmatrix} := K^\pi.$$

Thus, substituting $(I+G^\pi N^\pi)^{-1} = s(sI+G^\pi K^\pi)^{-1}$, (15) becomes

$$\begin{aligned}
&\lim_{s\to 0}s\left(sI+\bar{G}K^\pi\right)^{-1}\bar{G}\\
=&\lim_{s\to 0}s\begin{bmatrix}\left(sI+\operatorname{diag}(k_{p,i})K_{11}\right)^{-1} & \operatorname{diag}(k_{p,i})K_{12}\\ 0 & sI\end{bmatrix}^{-1}\begin{bmatrix}\operatorname{diag}(k_{p,i}) & 0\\ 0 & 0\end{bmatrix}\\
=&\lim_{s\to 0}s\begin{bmatrix}\left(sI+\operatorname{diag}(k_{p,i})K_{11}\right)^{-1} & \star\\ 0 & \frac{1}{s}I\end{bmatrix}\begin{bmatrix}\operatorname{diag}(k_{p,i}) & 0\\ 0 & 0\end{bmatrix}\\
=&\lim_{s\to 0}\begin{bmatrix}s\left(sI+\operatorname{diag}(k_{p,i})K_{11}\right)^{-1}\operatorname{diag}(k_{p,i}) & 0\\ 0 & 0\end{bmatrix}
\end{aligned}$$

which yields the required structure.

D. GFM Modeling Equations

The nonlinear differential-algebraic equations (DAEs) describing the GFM dynamics are given below in per units. The notation for variables and parameters is explained herein.

1) Differential Equations:

$$\begin{aligned}
\dot{\theta} &= \omega_b\delta\omega\\
\tau_\omega\dot{\delta\omega} &= -\delta\omega+(p^*-p)k_p\\
\tau_v\dot{\delta|v|} &= -\delta|v|+(q^*-q)k_q
\end{aligned}$$

2) Algebraic Equations:

$$\begin{aligned}
\delta\omega &= \omega-\omega_0\\
\delta|v| &= |v|-|v_0|\\
p &= v_{\mathrm{D}}i_{\mathrm{D}}+v_{\mathrm{Q}}i_{\mathrm{Q}}\\
q &= v_{\mathrm{Q}}i_{\mathrm{D}}-v_{\mathrm{D}}i_{\mathrm{Q}}\\
|v| &= \sqrt{v_{\mathrm{D}}^2+v_{\mathrm{Q}}^2}\\
v_{\mathrm{D}}\sin\theta &= v_{\mathrm{Q}}\cos\theta
\end{aligned}$$

Here, τ_ω & τ_v represent frequency & voltage filter time constants, and k_p & k_q denote the frequency & voltage droop gains, respectively. In contrast, $|v_0|$, ω_0 & ω_b denote the nominal voltage, angular frequency setpoint & base frequency of the inverter. Furthermore, v_{D} & v_{Q} refers to the global D- and Q-axis output voltage at PCC, while i_{D} & i_{Q} refers to the global D- and Q-axis output current at PCC, respectively. θ_c denotes the PCC angle w.r.t a global DQ-frame. The reference frames are illustrated in Fig. 6.

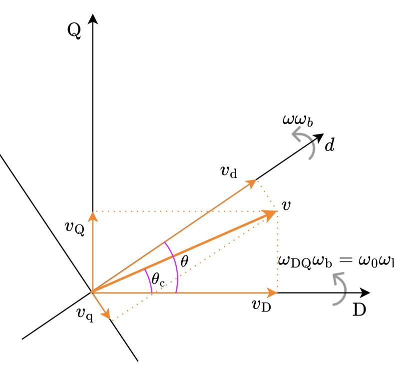

Fig. 6: Phasor diagram and reference frames of the GFM IBR.

I. Review #35A

A. Paper summary

The paper develops scalable small-signal stability certificates for networks of droop controlled converters that explicitly account for the network operating point (i.e., dispatch). The main result are stability conditions that are scalable in the sense that they can be verified for each converter by using information of neighboring converters. The conditions highlight that the network loading significantly impacts the stability region for the reactive power droop gain.

B. Comments for authors

Overall the paper makes an interesting and good contribution. The presentation is a bit hard to follow at times even for an expert reader because many mathematical concepts and choices (e.g., logarithmic voltage terms) are introduced without any discussion. While a full discussion of the results would obviously be challenging within the page limits of this conference, the presentation lacks clarity and precision at least on some aspects.

Overall, I would have expected a few more references and discussions of prior works with very similar conclusions. In decentralized analytical small-signal stability analysis the dispatch/power flow is indeed typically restricted to the trivial solution. In that sense, the authors address an important gap in the literature.

However, stability conditions obtained from nonlinear stability analysis that account for the effect of line loading and, in some cases losses, exist in the literature for GFM control (i.e., droop control, dispatchable virtual oscillator control, and complex droop control). These works have come to similar conclusions, i.e., reactive power line loading critically impacts stability regions for reactive power droop coefficients (see, e.g., Remark 5.11 in [R1]). While these conditions are typically not decentralized (i.e., depend on the algebraic connectivity of the network graph), they ultimately show the same relationship between (pair-wise) reactive loading of lossless static network models and bounds on reactive power-voltage droop coefficients.

Similarly, using logarithmic voltage terms is not new either (see, e.g., [R1]). Also, it appears that constant power loads are captured through the inputs (e.g., in Fig. 2a) but from the text of the paper itself this was not apparent to the reviewer.

The IBR dynamics used for analysis only capture the GFM control layer of IBRs but not other aspects (e.g., inner loops, output filters, active damping). While this is a fair assumption for a conference paper, not stating or discussing it is problematic. While the loop shifting approach and recovery of internal stability neatly addresses the problem that the network map is not passive in the usual inputs and outputs, it is unclear how cross coupling (i.e., arising from output filters) and lack of passivity of typical IBR dynamics (i.e., due to inner loops) impacts the results.

[R1] Schiffer, Ortega, Astolfi, Raisch, and Sezi, ”Conditions for stability of droop-controlled inverter-based microgrids”, Automatica, Volume 50, Issue 10, 2014

C. Summarize your recommendation in one to two sentences

Overall the paper makes an interesting and good contribution. The presentation is rather dense and could be improved, but overall this paper seems a good fit for this conference.

— *Anonymous reviewer*

II. Review #35B

A. Paper summary

The paper proposes a decentralised small-signal stability certificate for grids with grid-forming inverters, retaining explicit dependence on operating-point factors such as reactive-power imbalance and line loading, and using a loop-transformation passivity argument to derive local inequalities that guarantee stability; the main takeaway is that the permissible voltage-droop gains tighten as the network becomes more stressed, and this is illustrated on a two-bus example.

B. Comments for authors

The paper is generally well written. The primary contribution appears to be the replacement of common network-state simplifications in prior work with a framework that makes stability margins explicitly operating-point dependent and yields decentralised certificates without relying on hidden or nominal network-state assumptions. It would help explain and show what errors or overly optimistic/pessimistic margins arise when that network-state dependence is neglected or when restrictive operating-point assumptions are imposed, so as to more strongly motivate the study. The modelling choices are standard; the proof is classical (passivity + loop shifting) but executed in a way that exposes network-state parameters in the certificate. The combination of a port-based line model with integrators and a loop transformation with per-line diagonal shifts aggregated into bus-diagonal positive feedback, and a decentralised certificate that monotonically tightens with reactive mismatch and phase angle might be incrementally novel and practically insightful: as the mismatch in reactive power flowing in opposite directions on a line gets larger, and as the line becomes more heavily loaded, the range of voltage-droop gains that keep the system stable becomes smaller.

However, there are some comments for the authors to consider:

- It would help to state all simplifications and assumptions explicitly and up front; otherwise the work risks merely substituting one set of approximations for another. There are several simplifications and approximations applied throughout the paper, which are not clearly stressed and their implications discussed. The certificate relies on lossless lines and small-signal linearisation about a fixed operating point. This is typical for passivity-style certificates, but the lossless assumption should be discussed, as modest R/X ratios can change passivity of lines and the signs in Je. Currently, the assumption is stated (purely inductive line) but its implications/limitations are not deeply discussed.
- The paper adopts a first-principles small-signal model of GFMs interconnected by lossless, purely inductive lines. This is a widely used and sensible approximation for transmission level studies; however, again, it remains an approximation. For distribution feeders with non-negligible R/X, unbalances, and stronger P–V / Q–f cross couplings, the active–frequency / reactive–voltage decoupling implicit in the lossless formulation is weaker. The authors could briefly discuss how the framework could be extended to include resistive terms distribution-level coupling, or at least clarify the validity range of the present certificate. GFM inverters are expected to be ever more common across distribution networks.
- Section IV would benefit from clearer structure; as written, it reads like a self-contained mathematical exercise and loses sight of the paper's motivating questions. In particular, the claim that the per line loop shift acts locally while the induced diagonal term aggregates at buses appears to depend on the paper's simplifying assumptions. It would help clarify how realistic this decomposition is in practical networks, and delineate the conditions under which the locality/aggregation property continues to hold (or fails) beyond the idealised setting.
- The authors should specify which software environment or simulation tool was used to produce the numerical results. The validation relies on the GFM equations given in Appendix D and on their linearisation, but no reference is provided for the underlying implementation, and no high-fidelity simulation platform is mentioned, making it difficult to assess the reproducibility of the results.
- A 2-bus system is maybe too small to establish decentralised scalability or performance under meshed, multi line interactions. A larger, meshed network could be included and demonstrate how de are chosen per line, the certified region vs. eigenvalue maps, and how the margin shrinks under progressive loading / reactive mismatch.
- The paper shows its certificate working on a single illustrative case, but it does not systematically check, across many different operating points, whether the certificate's pass/fail decision is consistent with a higher fidelity "truth" method (for instance, computing the eigenvalues of the full linearised device plus network model at each operating point to see if all modes are stable, and running detailed time domain simulations to observe whether perturbations actually decay). It is hard to quantify how conservative the certificate is, how often it rejects operating points that are in fact stable, or whether it ever passes a point that turns out unstable, so adding that benchmarking would make the practical accuracy and safety of the proposed test transparent to readers. The paper could test robustness of the inequalities to measurement error and to moderate line resistances (e.g., sensitivity study: how much violation of "lossless" can be tolerated).

C. *Summarize your recommendation in one to two sentences*

The paper is generally well written with a potentially useful, operating-point-aware decentralised certificate, but the contribution is incrementally novel and currently under-validated. It would be needed to (i) state assumptions explicitly and discuss limitations, (ii) add meshed-network benchmarking and robustness analyses, and (iii) discuss parameter selection and implementation details.

— *Alessandra Parisio*

III. Review #35C

A. *Paper summary*

The paper derives decentralized stability certificates for a network of grid forming converters with frequency and voltage droop control. The key idea for proving internal stability is to show that the system can be expressed as the feedback interconnection of passive transmission lines with strictly passive converters. However, as the transmission line dynamics may not be passive in general, a loop transformation technique is employed to ensure internal stability. A two bus numerical example successfully illustrates the proposed method.

B. *Comments for authors*

The use of the loop transformation technique to establish internal stability despite a possible lack of passivity in the transmission line dynamics is a clever idea that was well executed in the paper. The resulting decentralized stability condition is very general and does not require simplifying assumptions such as small angle approximation or constant voltage magnitudes, and thus represents a substantial contribution beyond most existing work.

Several questions and comments:

1) The analysis appears to be quite specialized to the setting where all devices in the network are grid forming converters with frequency and voltage droop control. Is there any possibility of recovering similar decentralized stability certificates in more general settings, such as for other grid forming control design methods, and for heterogeneous networks that may also include generators, loads, grid following converters, etc?
2) The goal is to develop decentralized stability certificates as an alternative to, for example, direct eigenvalue analysis. However, the certificate in Theorem 3 relies on determining edge weights d_e for all transmission lines throughout the network. Even if candidate droop gains $k_{q,i}$ have already been determined, to check if these gains result in internal stability requires solving for a feasible set of $\{d_e\}$. How would one solve for such $\{d_e\}$ in practice, and how would the computational cost compare to distributed methods for computing eigenvalues directly?
3) Related to #2, could the proposed stability certificate be used to determine a priori sets of $\{k_{q,i}\}$ (for example, ranges of admissible $\{k_{q,i}\}$) which would result in internal stability? If so, how could this be done efficiently?
4) It was claimed that reactive power asymmetries progressively restrict the set of stabilizing voltage droop gains. However, for large θ_{ij}, in Eq. 5 it may be necessary to choose $\bar{d}_e > 1/cos(\theta_{ij})$, in which case it appears that larger reactive power asymmetries actually enlarge the set of stabilizing droop gains. Is this accurate for the true small signal stability (or just an undesirable property of the proposed stability certificate) and, if so, do you have any intuition for why this occurs?
5) Part of the motivation for decentralized stability certificates is to derive scale-free conditions for guaranteeing stability. However, the numerical example contains only two buses and, therefore, does not illustrate this scalability in practice. Moreover, it is unclear whether the lack of conservatism in the certificate that was observed for this example will generalize to other (and, in particular, larger) networks. Therefore, it may be valuable to include an example with a larger network.

Minor:

1) In IV.B.2, should be I_θ^{-1} instead of I_θ.
2) In figure 6, stable and unstable are reversed in the legend.
3) Why use log $|v|$ rather than $|v|$ throughout the paper? It also seems inconsistent with the model provided in Appendix D.

C. *Summarize your recommendation in one to two sentences*

The paper makes clever use of the loop transformation technique to derive decentralized stability certificates for networks of grid forming converters without requiring many simplifying but less accurate assumptions employed in the literature. Thus, it represents a substantial contribution, and I recommend it for publication and presentation at the conference.

— *Michael Fisher*

IV. Brief response to reviewers (optional)

V. Brief summary of changes made to the final paper

1) The main stability theorem was reformulated to ensure strict passivity of the loop-shifted Q–v channel. In particular, the nodal loop-shifting gains are now chosen to satisfy $\sum_{e:i\in e} d_e = \frac{1}{k_{q,i}}$, which makes the transformed voltage-channel dynamics strictly passive.
2) The equivalence of internal stability between the original feedback interconnection $H_1(s) \# H_2(s)$ and the loop-transformed interconnection $H_1'(s) \# H_2'(s)$ was clarified. Twas clarified. The classical loop-transformation argument usually requires no pole-zero cancellations on the *closed* right-half plane. This condition does not apply to our system because it has a pole-zero cancellation on the imaginary axis. We therefore added Lemma 2, together with Lemma 1, to establish the required internal-stability equivalence.
3) The case study was updated to include a point corresponding to an unstable parameter setting. This makes the numerical illustration show both a certified stable point and a point that violates the proposed stability condition.
4) The legend in the time-domain simulation was corrected so that the stable and unstable trajectories are labeled consistently.